Hindawi
Advances in Civil Engineering
Volume 2020, Article ID 9891825, 18 pages
https://doi.org/10.1155/2020/9891825

Research Article

Roadway Surrounding Rock under Multi-Coal-Seam Mining: Deviatoric Stress Evolution and Control Technology

Dongdong Chen,[1,2] **En Wang**,[1] **Shengrong Xie**,[1,3] **Fulian He**,[1] **Long Wang**,[1] **Qing Zhang**,[1] **Xiaoyu Wu**,[1] **Zaisheng Jiang**,[1] **Yubo Li**,[1] **and Songhao Shi**[1]

[1]*School of Energy and Mining Engineering, China University of Mining & Technology (Beijing), Beijing 100083, China*
[2]*State Key Laboratory of Mining Response and Disaster Prevention and Control in Deep Coal Mines, Anhui University of Science and Technology, Huainan 232001, China*
[3]*Beijing Key Laboratory for Precise Mining of Intergrown Energy and Resources, China University of Mining & Technology (Beijing), Beijing 100083, China*

Correspondence should be addressed to En Wang; wang_en1994@126.com and Shengrong Xie; xsrxcq@163.com

Received 15 February 2020; Revised 23 August 2020; Accepted 3 November 2020; Published 24 November 2020

Academic Editor: Valeria Vignali

Multi-coal-seam mining creates surrounding rock control difficulties, because the mining of a coal face in one seam can affect coal faces in another. We examine the effects of multi-coal-seam mining on the evolution of the deviatoric stress distribution and plastic zone in the roadway surrounding rock. In particular, we use numerical simulation, theoretical calculation, drilling detection, and mine pressure observation to study the distribution and evolution characteristics of deviatoric stress on Tailgate 8709 in No. 11 coal seam in Jinhuagong mine when the N8707 and N8709 coal faces in No. 7-4 coal seam and the N8707 and N8709 coal faces in No. 11 coal seam are mined. The evolution laws of deviatoric stress and the plastic zone of roadway surrounding rock in the advance and behind sections of the coal face are studied, and a corresponding control technology is proposed. The results show that the peak value of deviatoric stress increases with the advance of the coal face, and the positions of the peak value of deviatoric stress and the plastic zone become deeper. The deflection angle of the peak stress after mining at each coal face and the characteristics of the peak zone of deviatoric stress and the plastic zone of the roadway surrounding rock under the disturbance of multi-coal-seam mining are determined. In conclusion, the damage range in the roadway roof in the solid-coal side and coal pillar is large and must be controlled. A combined support technology based on high-strength and high pretension anchor cables and truss anchor cables is proposed; long anchor cables are used to strengthen the support of the roadway roof in the solid-coal side and coal pillar. The accuracy of the calculated plastic zone range and the reliability of the combined support technology are verified through drilling detection and mine pressure observation on site. This research can provide a point of reference for roadway surrounding rock control under similar conditions.

1. Introduction

Multi-coal-seam mining is common in China [1, 2], where coal seams that are shallow or have good mining conditions are nearly depleted in a short service life with the continuous increase in coal mining intensity [3]. During the downward mining of multiple coal seams, the supporting pressure above the residual coal pillars in the upper section and the collapsed roof in the gob will cause damage to the floor, which is now affected not only by the original rock stress but also by mining stress. Over time, the concentration, transmission, and change of stress in the floor due to multi-coal-seam mining will affect the panel of the lower coal seam, and it will become significantly more difficult to control the surrounding rock of the roadway [4, 5]. Much valuable research has been conducted on developing mechanisms and technology for the control of surrounding rock influenced by multi-coal-seam mining in recent years. For example, Zhu et al. [6] proposed a classification criterion for gob caving under multi-coal-seam mining conditions based in part on

the specifics of the interior load-bearing structures. Tan et al. [7] studied the failure characteristics of the upper strata after multi-coal-seam mining and showed that when the mining height of the lower coal seam is large, the strata of the upper coal seam have many fractures. Li et al. [8] detected the development of cracks in the floor of the upper coal seam after the mining of the lower coal seam. Qiang et al. [9] used a geographic information system to evaluate the likelihood of water inrushes and showed that different coal seams have different vulnerabilities in multiseam mining conditions. Zhang et al. [10] addressed the peak stress and influence-zone location for concurrent pillar recovery in two coal seams with 21 m of interburden at an approximate depth of 305 m. Deutsch and Wilde [11] modeled multiple coal seams in three dimensions without surface-contour or isochore mapping. Shang et al. [12] investigated the chain pillar and gateroad failure process, in which there is an increase in stress in the lower coal seam caused by a residual coal pillar in the upper coal seam.

According to the theory of plastic mechanics, the surrounding-rock stress is the superposition of spherical stress and deviatoric stress. The deviatoric stress is the root cause of the distortion of the roadway surrounding rock, and it plays a major role in the occurrence and development of plastic deformation [13, 14]. There have been several observational and theoretical studies of the distribution of the deviatoric stress and the plastic zone of roadway surrounding rock. For example, Ma et al. [15] applied the Mohr-Coulomb criterion to obtain the deviatoric stress formula for circular-roadway surrounding rock in a nonuniform stress field. Xu et al. [16, 17] simulated the deviatoric stress distribution in ultrahigh roadway and under abandoned coal pillars in multi-coal-seam mines. Yu et al. [18] deduced the analytical form of the deviatoric stress field of surrounding rock from rock mechanics and other related theories and analyzed the distribution of surrounding rock under different conditions. He et al. [19] investigated the roof deviatoric stress, surrounding-rock fracture field, and deformation law when changing the width of a large-section open-off cut roof from 6 to 10 m. Xie et al. [20, 21] adopted a strain-softening model to simulate the deviatoric stress evolution laws of surrounding rock at gob-side entry retaining throughout the whole process of the coal face's advance.

Most existing research on roadway surrounding-rock failure in multi-coal-seam mining has focused on the vertical or horizontal stresses. There has been no targeted study on the distribution law of deviatoric stress in roadway-floor surrounding rock disturbed by multi-coal-seam mining. This paper considers the effect of multi-coal-seam mining on Tailgate 8709 in Jinhuagong mine, Datong City, Shanxi Province, China. The FLAC^{3D} numerical calculation software is used to study the disturbance mechanisms, deviatoric stress, and plastic zones of the N8707 coal face and the N8709 coal face in No. 7-4 coal seam and the N8707 coal face and the N8709 coal face in No. 11 coal seam. The peak deviatoric stress profile and plastic zone profile of the roadway surrounding rock are determined, and a combined support technology using high-strength and high pretension anchor cables and truss anchor cables is proposed for Tailgate 8709. The accuracy of the plastic zone and the reliability of the combined support technology are verified by arranging on-site drilling detection and mine pressure observation. This research can provide a point of reference for the control of surrounding rock similarly disturbed by multi-coal-seam mining.

2. Project Overview

Jinhuagong coal mine is a short distance west of Datong City, Shanxi Province, China. It is a typical multi-coal-seam mine with complex geological conditions. The thicknesses of No. 7-4, No. 11, and No. 12 coal seams in Jinhuagong mine are 1.4 m, 3.3 m, and 2.1 m, respectively. The vertical distance between No. 7-4 and No. 11 coal seams is 38.8 m, and that between No. 11 and No. 12 coal seams is 19.9 m. At present, No. 7-3 coal seam has been mined out, and Headgate 8707 and Tailgate 8709 in No. 11 coal seam have been excavated. The N8707 and N8709 coal faces in No. 7-4 coal seam and the N8707 and N8709 coal faces in No. 11 coal seam are being mined as planned. The average burial depth of No. 11 coal seam is about 300 m, and the average dip angle is 3°. The roof and floor lithologies of No. 11 coal seam and the mining sequence of each coal face are shown in Figure 1.

3. Numerical Simulation of Tailgate 8709 under Multi-Coal-Seam Mining

3.1. Numerical Model. The FLAC^{3D} numerical simulation software has been used to construct a mathematical model of Tailgate 8709 in No. 11 coal seam in Jinhuagong mine under multi-coal-seam mining. The model is visualized in Figure 2. We simulate each rock layer using the Mohr-Coulomb constitutive model, the one most widely used in FLAC^{3D} numerical simulation of various rock formations. Following [22–31], we use a strain-softening model to simulate the mechanical behavior of coal seams. Like [32–39], we use the natural collapse method to deal with the gob of the coal face in the simulation. The coal face in the model is taken to extend 200 m along the x-axis. The y-axis represents the advancing direction of the coal face, taken to extend 120 m, and the z-axis is the vertical direction, taken to extend 140 m. The size of the model is thus 200 m × 120 m × 140 m. Because various joints and cracks often exist in the rock mass on-site, the rock mechanical parameters measured in laboratory tests are significantly higher than the actual parameters in the field; laboratory results cannot be used directly as the mechanical parameters of each rock layer in the model. Based on the Hoek-Brown failure criterion [40, 41], the laboratory test results are calculated and processed to obtain the mechanical parameters of various rock masses listed in Table 1.

The mining process of the simulated coal face is required to be consistent with the actual mining sequence at Jinhuagong mine; that is, the N8707 and N8709 coal faces in No. 7-4 coal seam and the N8707 and N8709 coal faces in No. 11 coal seam are mined in the stated order. In the simulation, the excavation step is set as 5 m. Nephograms of the deviatoric stress in the roadway surrounding rock at

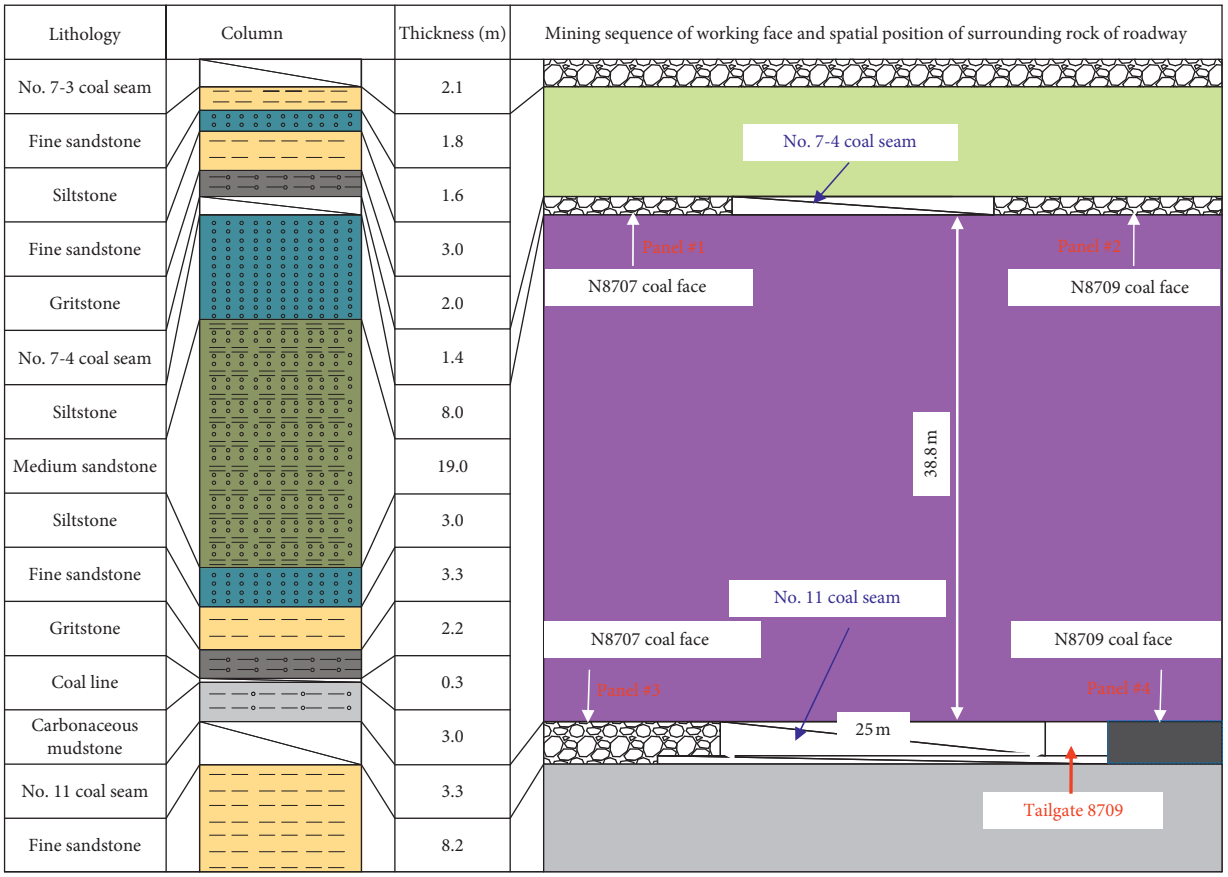

Figure 1: Lithology of the coal seam and mining sequence of each coal face.

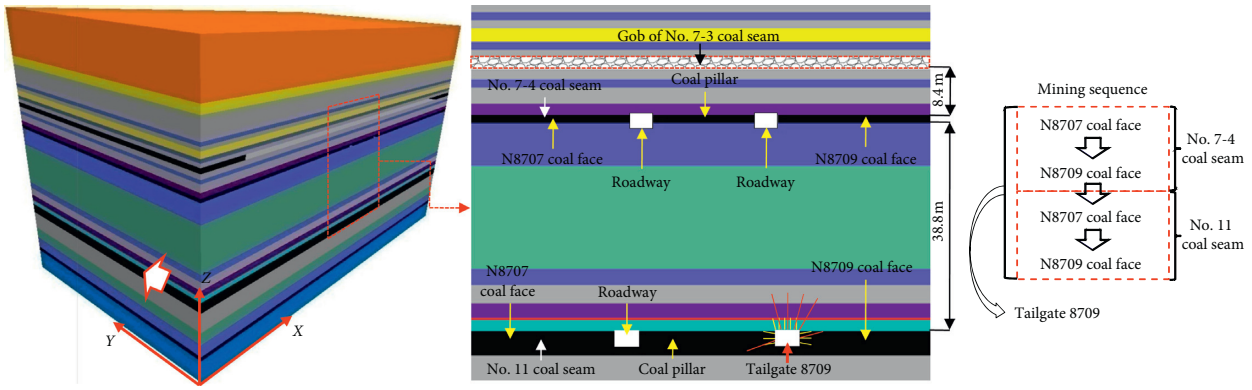

Figure 2: Numerical model and roadway layout.

different stages are analyzed, and deviatoric stress data is extracted to draw stress curves. The disturbances to Tailgate 8709 in No. 11 coal seam caused by multi-coal-seam mining are explored with nephograms of deviatoric stress and models of the plastic zone distribution.

3.2. The Strain-Softening Model and Its Parameters. The plastic shear strain parameter ε^{ps} of coal after yielding used in the strain-softening criterion is

$$\varepsilon^{ps} = \left\{\frac{1}{2}\left[\left(\varepsilon_1^p - \varepsilon_m^p\right)^2 + \left(\varepsilon_m^p\right)^2 + \left(\varepsilon_3^p - \varepsilon_m^p\right)^2\right]\right\}^{(1/2)}, \quad (1)$$

where ε_1^p and ε_3^p are the plastic principal strain components, and

$$\varepsilon_m^p = \frac{1}{3}\left(\varepsilon_1^p + \varepsilon_3^p\right). \quad (2)$$

The strain-softening model employs the Mohr-Coulomb yield criterion [42]:

Table 1: Mechanical parameters of rock strata and coal seams.

Lithology	Bulk modulus (GPa)	Shear modulus (GPa)	Cohesion (MPa)	Tensile strength (MPa)	Internal friction angle (°)	Density (g/cm^3)
Medium sandstone	7.50	4.10	1.60	6.51	34	2.70
Fine sandstone	5.32	2.84	1.46	5.54	31	2.65
Siltstone	5.82	3.14	1.30	5.70	32	2.55
No. 7-3 coal seam	3.75	1.87	1.10	0.95	27	1.40
Gritstone	9.32	6.50	1.86	7.58	35	2.82
No. 7-4 coal seam	3.75	1.87	1.10	0.95	27	1.40
Sandy mudstone	4.28	2.30	1.20	1.19	28	2.36
No. 11 coal seam	3.75	1.87	1.10	0.95	27	1.40

$$\sigma_1 = \frac{1+\sin\varphi(\varepsilon^{ps})}{1-\cos\varphi(\varepsilon^{ps})}\sigma_3 + \frac{2c(\varepsilon^{ps})\cos(\varphi(\varepsilon^{ps}))}{1-\sin(\varphi(\varepsilon^{ps}))}, \quad (3)$$

where σ_1 and σ_3 are the maximum and minimum principal stresses, respectively; $\varphi(\varepsilon^{ps})$ is the friction angle after plastic failure:

$$\varphi(\varepsilon^{ps}) = \begin{cases} \varphi_p, & \varepsilon^{ps} \le \varepsilon_p, \\ \dfrac{\varphi_r - \varphi_p}{\varepsilon_r - \varepsilon_p}\left(\varepsilon^{ps} - \varepsilon_p\right) + \varphi_p, & \varepsilon_p < \varepsilon^{ps} < \varepsilon_r, \\ \varphi_r, & \varepsilon^{ps} \ge \varepsilon_p. \end{cases} \quad (4)$$

and $c(\varepsilon^{ps})$ is the cohesion after plastic failure:

$$c(\varepsilon^{ps}) = \begin{cases} c_p, & \varepsilon^{ps} \le \varepsilon_p, \\ \dfrac{c_r - c_p}{\varepsilon_r - \varepsilon_p}\left(\varepsilon^{ps} - \varepsilon_p\right) + c_p, & \varepsilon_p < \varepsilon^{ps} < \varepsilon_r, \\ c_r, & \varepsilon^{ps} \ge \varepsilon_p. \end{cases} \quad (5)$$

ε_r is the plastic strain in the residual stage;
ε_p is the plastic strain at the peak stress;
φ_p is the friction angle at the peak stress;
c_p is the cohesion at the peak stress;
φ_r is the friction angle in the residual stage;
c_r is the cohesion in the residual stage.

The strain-softening parameters ε (plastic strain), φ (friction angle), and c (cohesion) were determined through laboratory uniaxial compression testing (Table 2).

In order to verify the rationality of adopting a strain-softening model for the coal seam in the FLAC^{3D} software, a standard cylinder test piece, $\Phi 50 \times 100$ mm, was fabricated, and a load was uniformly applied to its upper part at a constant rate until the test piece was damaged. This experiment was then simulated using FLAC^{3D}. Figure 3 shows that the stress-strain curves from laboratory experiment and numerical simulation are consistent, indicating that it is reasonable to use a strain-softening criterion in the model.

Table 2: Parameter of cohesion and friction angle as functions of plastic strain.

ε	φ (°)	c (MPa)
0	25.0	1.80
0.008	22.0	1.60
0.095	12.0	0.45
0.012	7.0	0.15

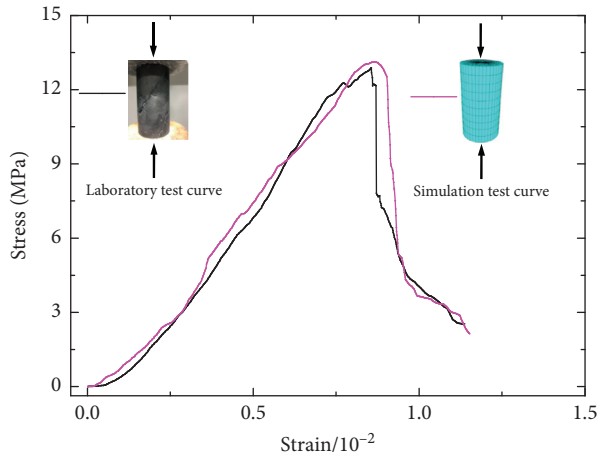

Figure 3: Stress-strain curves of laboratory test and simulation.

3.3. Distribution and Evolution Characteristics of Deviatoric Stress in Roadway Surrounding Rock Affected by Multi-Coal-Seam Mining. In order to study the disturbance of the N8707 and N8709 coal faces in No. 7-4 coal seam on the N8707 and N8709 coal faces in No. 11 coal seam on Tailgate 8709, the distribution and evolution laws of deviatoric stress and the plastic zone of the roadway surrounding rock in the mining process of each coal face are studied.

3.3.1. Overview of Deviatoric Stress. When the surrounding rock in a coal mine is in a state of hydrostatic pressure, the principal stresses σ_i $(i = 1, 2, 3)$ are perpendicular to each

other and equal in value: $\sigma_1 = \sigma_2 = \sigma_3$. The rock stress in the roadway will change after the roadway is excavated, and the following relationship applies: $\sigma_1 \geq \sigma_2 \geq \sigma_3$. It can also be shown that

$$\begin{pmatrix} \sigma_1 - \sigma_m & 0 & 0 \\ 0 & \sigma_2 - \sigma_m & 0 \\ 0 & 0 & \sigma_3 - \sigma_m \end{pmatrix} + \begin{pmatrix} \sigma_m & 0 & 0 \\ 0 & \sigma_m & 0 \\ 0 & 0 & \sigma_m \end{pmatrix} = \begin{pmatrix} \sigma_1 & 0 & 0 \\ 0 & \sigma_2 & 0 \\ 0 & 0 & \sigma_3 \end{pmatrix}, \tag{6}$$

where σ_m is the average stress: $\sigma_m = (1/3)\sum_{i=1}^{3} \sigma_i$.

The deformation of an object is caused by changes in its volume and shape. The second term on the left side of formula (6) is the spherical stress tensor, which causes changes in volume, while the first item is the deviatoric stress tensor, which causes changes in shape (plastic deformation and failure). The deviatoric stress is the essential cause of rock-mass failure. The principal deviatoric stress defined as $\sigma_i - \sigma_m$ in the above formula is principal deviatoric stress. The maximum principal deviatoric stress (σ') is therefore given by

$$\sigma' = \sigma_1 - \sigma_m = \sigma_1 - \frac{\sigma_1 + \sigma_2 + \sigma_3}{3}. \tag{7}$$

The shear stress of the shallow surrounding rock in the roadway is concentrated after the roadway is excavated, and the surrounding rock releases energy, unloading deformation. The deviatoric stress is a combination of horizontal, vertical, and tangential stress that can be used to characterize the distribution of shear stress, the essential source of rock deformation and failure, under the action of a load. The present research therefore highlights deviatoric stress as an index reflecting the failure evolution of surrounding rock more comprehensively than does vertical or horizontal stress alone.

3.3.2. The Deviatoric Stress Distribution of Tailgate 8709 under the Mining of the N8707 and N8709 Coal Faces in No. 7-4 Coal Seam. Figure 4 shows the deviatoric stress distributions after the N8707 and N8709 coal faces in No. 7-4 coal seam have been mined. It can be seen from Figure 4(a) that an approximately "fan shaped" peak zone of deviatoric stress is formed at the right coal-pillar boundary after the N8707 coal face in No. 7-4 coal seam is mined out and that the deviatoric stress gradually decreases away from the peak zone. The surrounding rock of Tailgate 8709 in No. 11 coal seam also has a peak zone of deviatoric stress (concentrated mainly in the roof and floor), and the stress of the roadway surrounding rock has an approximately symmetrical distribution; this shows that the roadway is not obviously affected by the mining disturbance of the N8707 coal face in No. 7-4 coal seam. Because Tailgate 8709 in No. 11 coal seam is 38.8 m below the N8709 coal face in No. 7-4 coal seam, it is far away from the N8707 coal face in No. 7-4 coal seam and is therefore not significantly disturbed by the mining of the N8707 coal face in the upper coal seam.

Figure 4(b) shows that an approximately symmetrical "八" shaped peak zone of deviatoric stress, with the left and right sides of coal pillars as the boundary, is formed after both sides of the coal pillar in No. 7-4 coal seam are mined. The stress value below the peak zone of deviatoric stress falls off slowly. The peak zone of deviatoric stress of Tailgate 8709 in No. 11 coal seam deflects obviously compared with Figure 4(a). The reason for this phenomenon is that Tailgate 8709 is located under the N8709 coal face in No. 7-4 coal seam, and the partial stresses of two overlap. The peak zone of deviatoric stress of the roadway surrounding rock deflects to the bottom corner on the coal-pillar side and the shoulder corner of the roadway roof on the solid-coal side.

Figure 5 shows that the distribution curves of deviatoric stress in the surrounding rock in solid coal, coal pillar, roof, and floor are approximately the same after the N8707 and N8709 coal faces in No. 7-4 coal seam are mined. The deviatoric stress of the roadway surrounding rock, especially of the roof, shows an increasing trend after the N8709 coal face in No. 7-4 coal seam is mined; the peak value of deviatoric stress of the roof (3.73 MPa after mining of the N8707 coal face) increases to 4.06 MPa after mining of the N8709 coal face. The farther one looks away from the roof of Tailgate 8709 in No. 11 coal seam, the more obvious is the increase of deviatoric stress. Therefore, it can be concluded that the deviatoric stress in surrounding rock of Tailgate 8709 in No. 11 coal seam is redistributed due to the fact that the N8709 coal face in No. 7-4 coal seam is mined combining with the deflection of the peak zone of deviatoric stress in roadway surrounding rock in Figure 4(b), which makes deviatoric stress of roadway surrounding rock gradually increase. After the N8709 coal face in No. 7-4 coal seam is mined, the peak distances of deviatoric stress in solid-coal side, coal pillar, and floor of Tailgate 8709 in No. 11 coal seam are about 2.0 m, 2.5 m, and 2.0 m, respectively. The peak distance of the roof after mining of the N8707 coal face increases from 2.5 m to 4.0 m after mining of the N8709 coal face. The roadway roof is the area most affected by mining of the coal face in the overlying coal seam.

3.3.3. The Deviatoric Stress Distribution of Tailgate 8709 under the Mining Disturbance of the N8707 Coal Face in No. 11 Coal Seam. Figure 6 shows nephograms of the deviatoric stress distribution of surrounding rock in the advance and behind sections of Tailgate 8709 when the N8707 coal face in No. 11 coal seam is mined for various distances. The nephograms and curves with positive numbers represent the advance sections and those with negative numbers the behind sections. It can be seen that the nephograms of deviatoric stress of Tailgate 8709 are approximately the same, which shows the rationality of leaving 25 m coal pillars between the N8707 coal face and the N8709 coal face in No. 11 coal seam. With a sufficient width of coal pillar, mining of the adjacent coal face has no great impact on Tailgate 8709. The peak zone of deviatoric stress is mainly at the shoulder corner of the roadway roof in solid coal and at the bottom corner of the coal pillar. The peak stress at the shoulder corner of the roadway roof in solid coal is far from the roadway surface, so it is necessary to strengthen the support for it in solid coal.

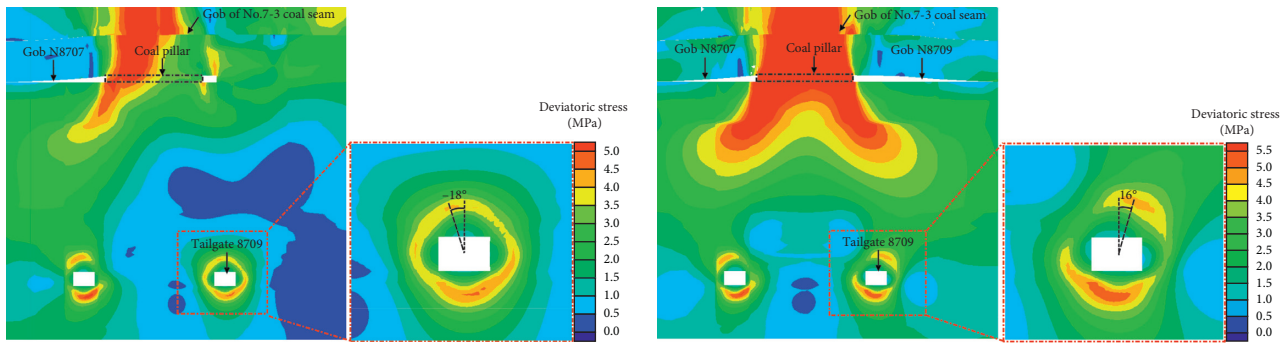

FIGURE 4: Nephograms of deviatoric stress after mining of N8707 and N8709 coal faces in No. 7-4 coal seam: (a) nephogram of deviatoric stress after mining of the N8707 coal face in No. 7-4 coal seam; (b) nephogram of deviatoric stress after mining of the N8709 coal face in No. 7-4 coal seam.

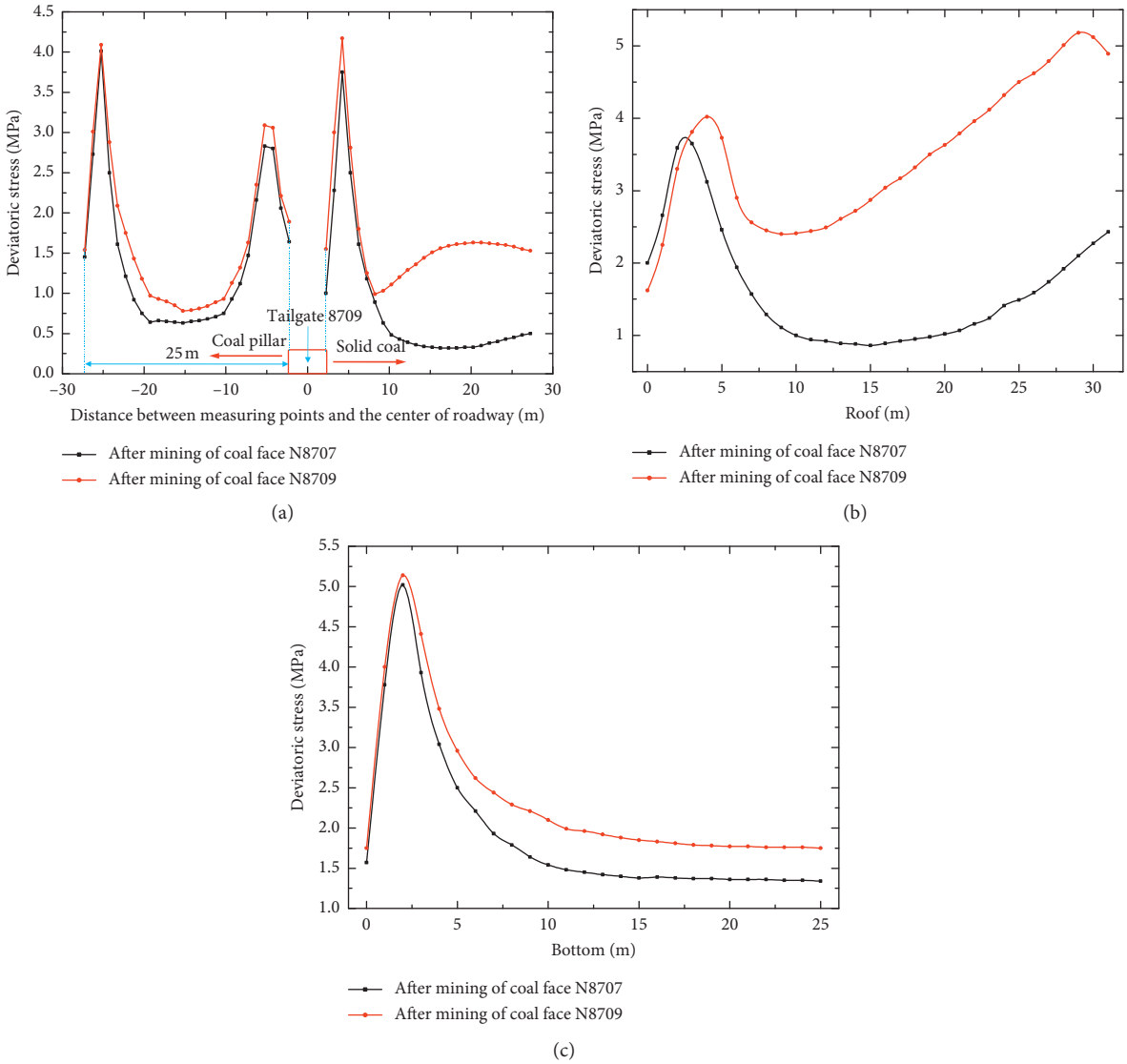

FIGURE 5: Deviatoric stress curves after mining of N8707 and N8709 coal faces in No. 7-4 coal seam: (a) deviatoric stress curves in coal pillar and solid-coal side; (b) deviatoric stress curves of the roof; (c) deviatoric stress curves of the bottom.

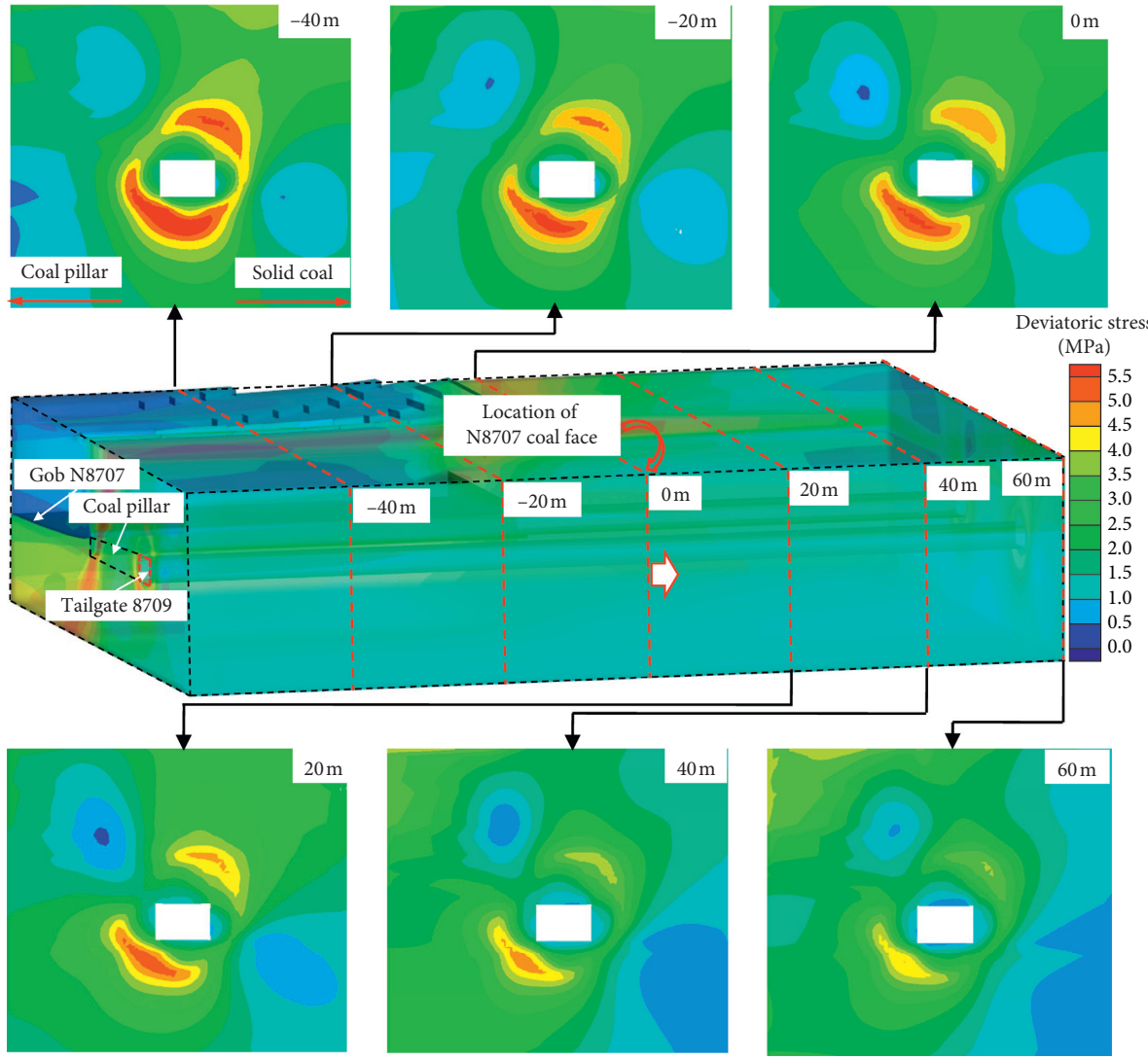

Figure 6: Nephograms of deviatoric stress of Tailgate 8709 in the mining process of the N8707 coal face in No. 11 coal seam.

Figure 7 shows that the deviatoric stress curves of the surrounding rock of Tailgate 8709 are approximately the same in the solid-coal side, coal pillar, roof, and floor after the mining of the N8707 coal face in No. 11 coal seam but that the deviatoric stress of surrounding rock of the advance and behind sections changes greatly. The main conclusion to be drawn is that the farther the behind coal face is, the greater the deviatoric stress of Tailgate 8709 is. That is, the deviatoric stress of roadway surrounding rock is greater than that of roadway surrounding rock at different positions in the advance section when the behind coal face is at a distance of 40 m. The peak values of deviatoric stress in the roof, solid coal, coal pillar, and floor of Tailgate 8709 at 40 m behind the coal face are about 4.11 MPa, 7.17 MPa, 5.60 MPa, and 4.75 MPa, respectively, and the distances between the peak stress locations and the roadway surface are about 4.0 m, 2.5 m, 4.0 m, and 2.5 m. In the advancing coal-face section, the deviatoric stress of Tailgate 8709 shows little change, which indicates that the mining of the N8707 coal face in No. 11 coal seam has little effect on deviatoric stress in the surrounding rock of Tailgate 8709 in the advance section, although it causes some disturbance in the deviatoric stress distribution of roadway surrounding rock in the behind coal-face section. The peak positions of deviatoric stress in solid coal, coal pillar, roof, and floor of roadway in the advance and behind sections exhibit no obvious changes. Therefore, Tailgate 8709 is hardly affected by the mining of the N8707 coal face in No. 11 coal seam, proving that it is reasonable to set a 25 m coal pillar between two adjacent coal faces. The deviatoric stresses at 2 m (in the shallow surrounding rock of the solid-coal side), 3 m (in the shallow surrounding rock of the coal pillar), and 4 m (in the shallow surrounding rock of the roof) show an increasing trend, which indicates that the shallow surrounding rock of the roadway is damaged to a certain extent and the deviatoric stress is low. Thus, it is necessary to control the stability of rock masses with fracture development in this range, while at the same time strengthening the support for the shoulder corner of the roadway roof on the solid-coal side.

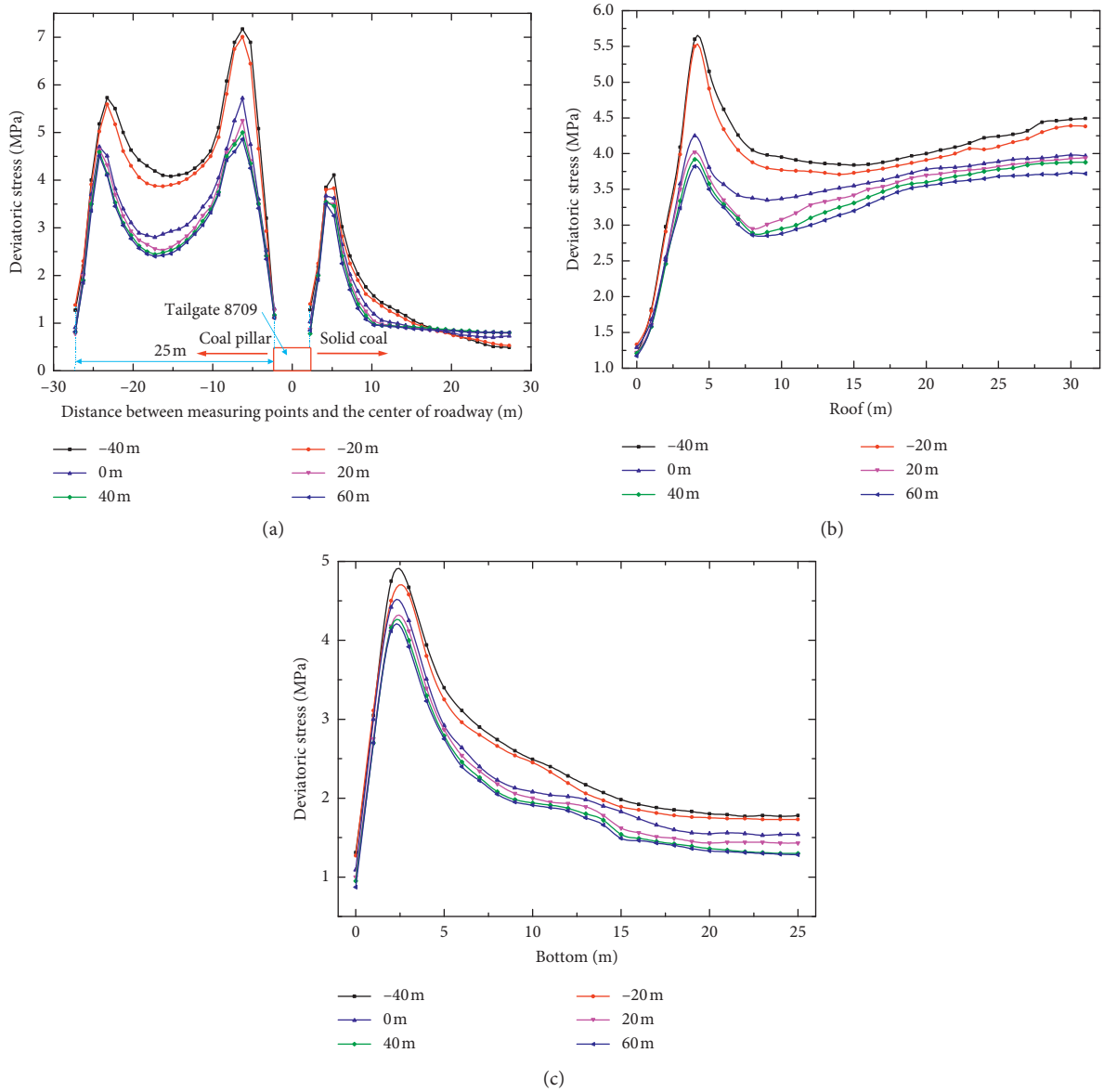

Figure 7: Deviatoric stress curves of Tailgate 8709 in the mining process of the N8707 coal face in No. 11 coal seam: (a) deviatoric stress curves in coal pillar and solid-coal side; (b) deviatoric stress curves of the roof; (c) deviatoric stress curves of the bottom.

3.3.4. The Deviatoric Stress Distribution of Tailgate 8709 under the Mining of the N8709 Coal Face in No. 11 Coal Seam. Figure 8 shows nephograms of deviatoric stress at different positions of the advanced region of Tailgate 8709 when the N8709 coal face in No. 11 coal seam is mined to various distances. It can be seen that the deviatoric stress of the surrounding rock of Tailgate 8709 increases rapidly when approaching the coal face gradually, and the roadway surrounding rock has an irregularly distributed peak zone of deviatoric stress. The position of the peak zone of deviatoric stress has been deflected and deepened compared with that in Figure 6, and the peak zone is stably distributed at the shoulder corner of the roadway roof on the solid-coal side and the bottom corner of the coal pillar.

According to Figure 9, the deviatoric stress curves of Tailgate 8709 in solid-coal side, coal pillar, roof, and floor differ at different positions of the advance coal face. Deviatoric stress values on the solid-coal side near the coal face gradually increase with depth. The deviatoric stress curves in this region rise at first, when the advance coal face is far away, then decrease, and finally tend to become flat. The deviatoric stress curves in the coal pillar show an "*M*" shape. The farther the advance coal face is, the less the deviatoric stress is. The deviatoric stress curves on the solid-coal side and in the coal pillar will gradually become coincident after 40 m advance of the coal face. This shows that, over this much advance of the coal face, the mining influence is gradually reduced, and the distribution of deviatoric stress tends to become stable. The deviatoric stresses of the roof and floor near the coal face are greatly affected by the mining of the coal face. The distance between the peak location of deviatoric stress of the roof and surface of the roof increases to 4.0 m, and the position of the

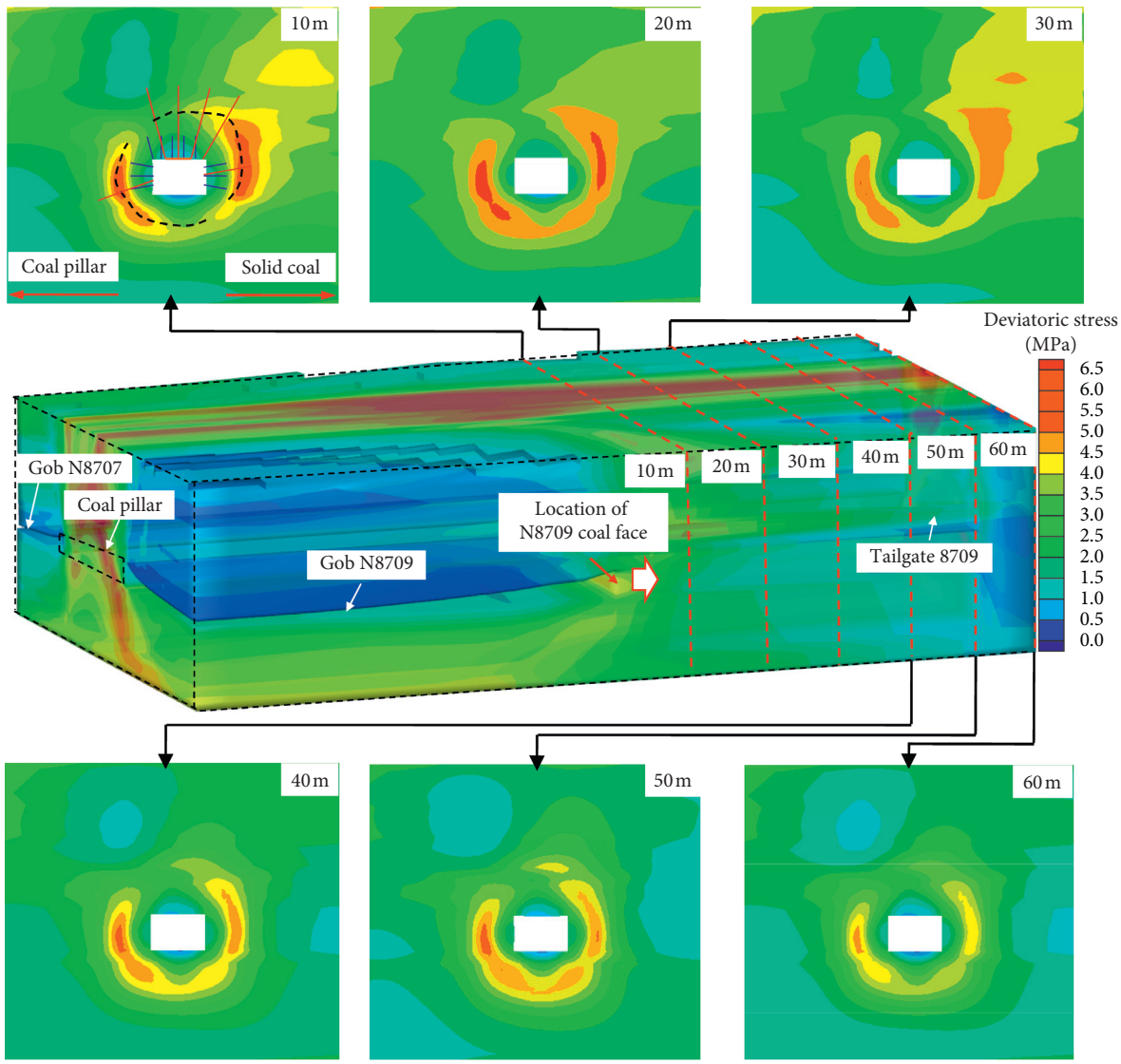

Figure 8: Nephograms of deviatoric stress of Tailgate 8709 in the mining process of the N8709 coal face in No. 11 coal seam.

peak value of deviatoric stress deepens. The distribution curves of deviatoric stress are almost coincident after 40 m advance of the coal face, and the distance between the peak location of deviatoric stress and the roof surface after stabilization is reduced to 4.0 m. The peak values of deviatoric stress in the solid-coal side, coal pillar, roof, and floor of Tailgate 8709 in the advanced coal face are about 5.85 MPa, 4.64 MPa, 5.20 MPa, and 5.23 MPa respectively, and the corresponding distances of the peak stress are 3.0 m, 4.0 m, 4.0 m, and 2.5 m. It is necessary to strengthen the reinforcement of roadway surrounding rock within this range during the support design.

3.4. Distribution and Evolution Laws of Plastic Zone in Tailgate 8709 under Multi-Coal-Seam Mining. Figure 10 shows nephograms of the deviatoric stress and the plastic zone of the surrounding rock in Tailgate 8709 after the mining of No. 7-4 and No. 11 coal seams. From the nephograms (Figure 10(a)), it can be concluded that the peak zone of deviatoric stress of the roof of the N8709 coal face in No. 7-4 coal seam is deflected by 34° from the peak zone of deviatoric stress of the surrounding rock in Tailgate 8709. The peak zone of deviatoric stress of the roof continues to be deflected by 13° after mining of the N8707 coal face in No. 11 coal seam, and the peak zone of deviatoric stress of the roof continues to be deflected by 53° when No. 11 coal seam is 10 m ahead of the N8709 coal face. Therefore, the peak zone of deviatoric stress of Tailgate 8709 continually deflects to find a new effective bearing structure after the roadway surrounding rock is damaged under the influence of multi-coal-seam mining. It should be ensured during the support design that the anchor cable can pass through the position of the peak zone of deviatoric stress (Figure 10(d)).

Figure 10(a) shows that the plastic zone of the surrounding rock of Tailgate 8709 is symmetrically distributed after the mining of the N8707 coal face in No. 7-4 coal seam, which shows that Tailgate 8709 in No. 11 coal seam is scarcely affected by the mining of the N8707 coal face in No. 7-4 coal seam. This is approximately consistent with the

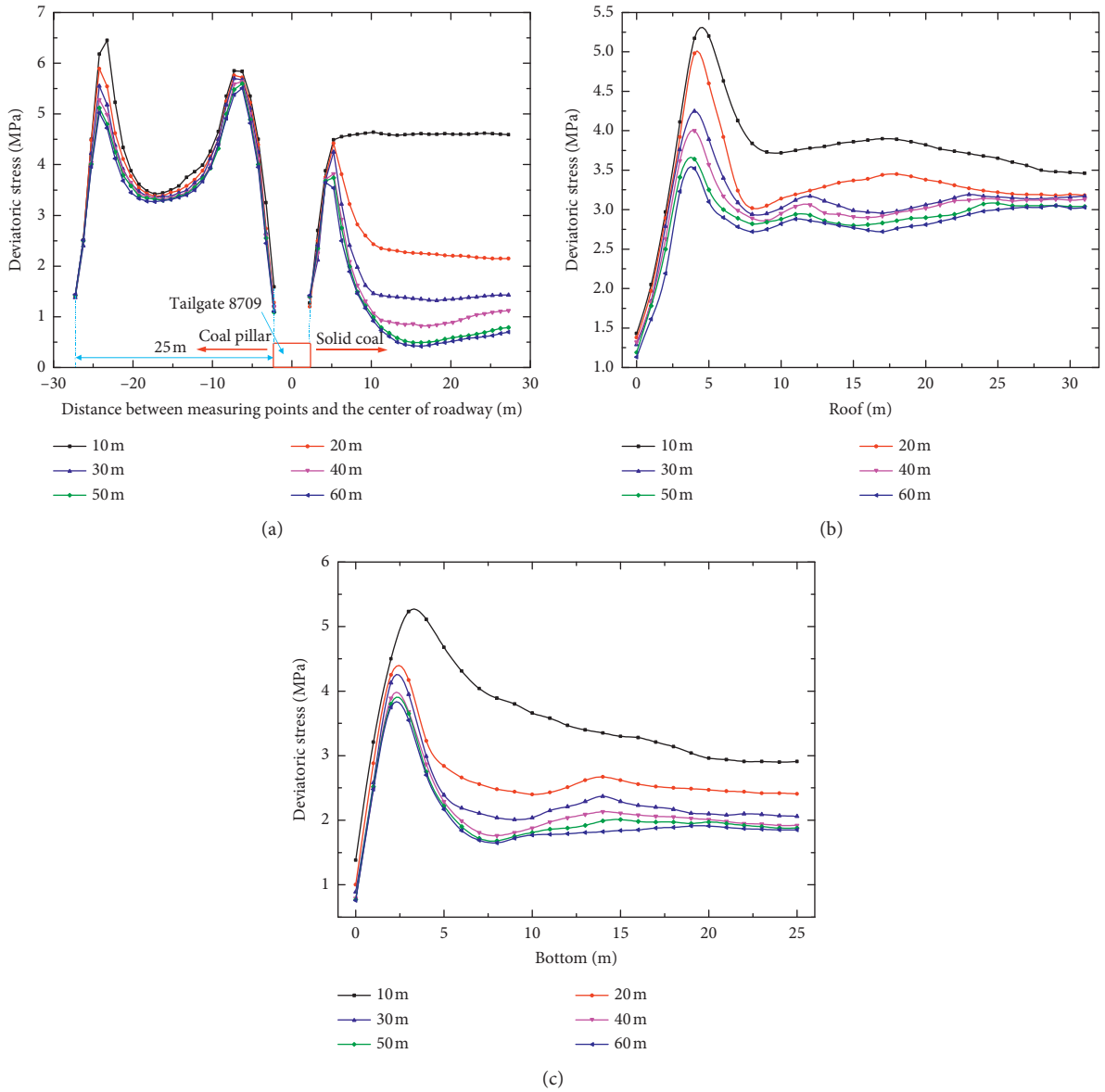

Figure 9: Deviatoric stress curves of Tailgate 8709 in the mining process of the N8707 coal face in No. 11 coal seam: (a) deviatoric stress curves in coal pillar and solid-coal side; (b) deviatoric stress curves of the roof; (c) deviatoric stress curves of the bottom.

distribution of the peak zone of deviatoric stress. The depths of the plastic zone on the roof, solid coal, coal pillar, and floor are about 3.0 m, 2.0 m, 2.0 m, and 2.0 m, respectively. Figure 10(b) shows that the plastic zone of the N8709 coal face in No. 7-4 coal seam is asymmetrical under the mining influence of the N8709 coal face in No. 7-4 coal seam, and the depths of the plastic zone in the roof, solid coal, coal pillar, and floor are about 3.5 m, 2.5 m, 2.5 m, and 2.5 m, respectively. The plastic zone of Tailgate 8709 continues to deflect in a clockwise direction as a result of the mining of the adjacent N8707 coal face, according to Figure 10(c). The plastic zone obviously increases its range and begins to deflect to the shoulder corner of the roadway roof in solid coal and to the floor corner of the coal pillar. The plastic zone of the roadway surrounding rock is obviously asymmetric. The depths of the plastic zone on the roof, solid-coal side, coal pillar, and floor are about 3.5 m, 2.5 m, 3.5 m, and 2.5 m, respectively. At this time, the distances between the peak zones of deviatoric stress and the roadway surface are about 4.0 m, 2.5 m, 4.0 m, and 2.5 m, respectively, and the ranges are approximately the same as those of the plastic zone. According to Figure 10(d), the plastic zone of roadway surrounding rock continues to expand and has an obviously asymmetric distribution when Tailgate 8709 is 10 m ahead of the coal face. The plastic zone in the shoulder corner of the roadway roof on the solid-coal side and in the coal pillar has a large expansion range, as does the deviatoric stress distribution there. The depths of the plastic zone on the roof, solid-coal side, coal pillar, and floor are about 4.0 m, 3.0 m, 3.5 m, and 3.0 m, respectively. The shallow surrounding rock of Tailgate 8709 mainly suffered shear failure and tensile failure under the disturbance of the mining face. Therefore,

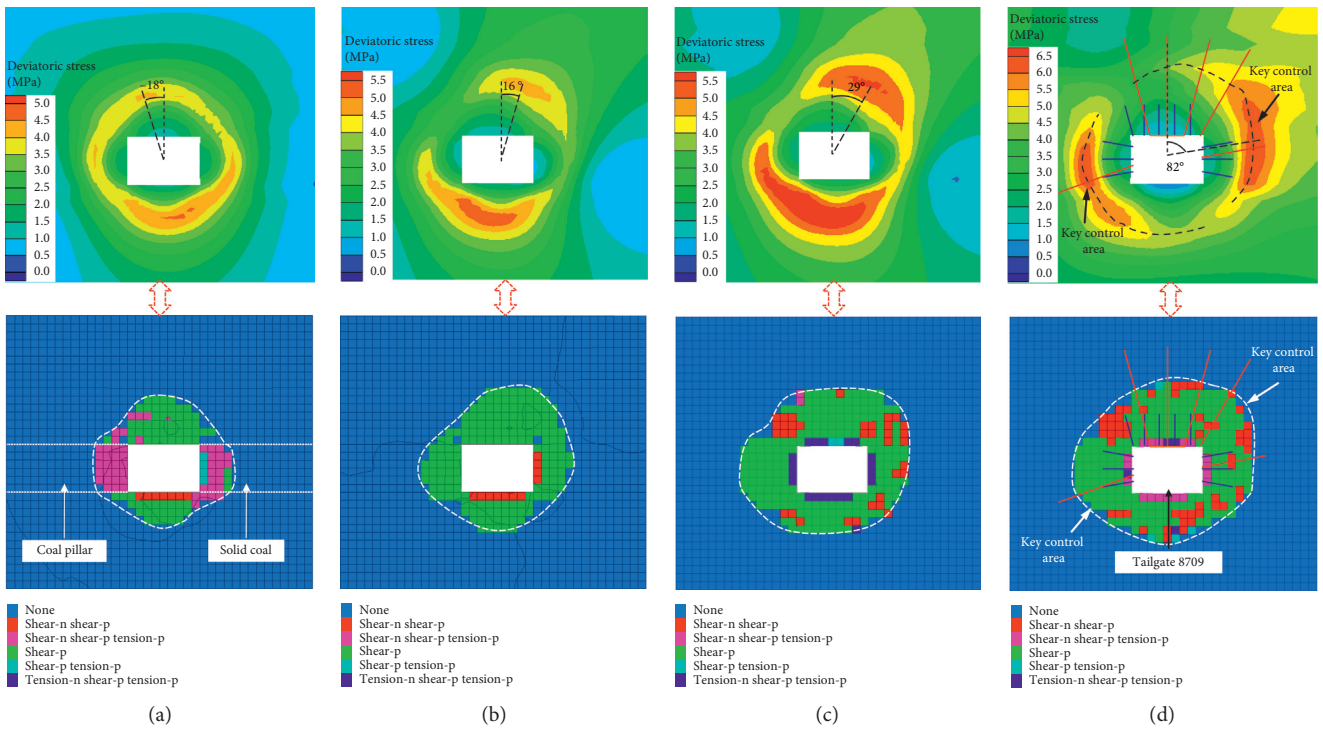

Figure 10: Nephograms of deviatoric stress and plastic zone of Tailgate 8709 under multi-coal-seam mining: (a) after mining of the N8707 coal face in No. 7-4 coal seam; (b) after mining of the N8709 coal face in No. 7-4 coal seam; (c) after mining of the N8707 coal face in No. 11 coal seam; (d) in the advance 10 m of the N8709 coal face in No. 11 coal seam.

in the control of roadway surrounding rock, it is necessary to ensure that the surrounding rock of shallow shear and tensile failure is anchored to the deep undamaged elastic coal and rock mass.

In summary, the plastic zone of Tailgate 8709 shows an obviously asymmetric distribution affected by multi-coal-seam mining. The shoulder corners of the roadway roof in solid-coal side and coal pillar are in a large range of plastic states. The maximum depths of the plastic zone on the roof, solid-coal side, coal pillar, and floor of Tailgate 8709 are about 4.0 m, 3.0 m, 3.5 m, and 2.5 m, respectively, and the plastic zone of the shoulder corner of the roadway roof on the solid-coal side extends up to 4.0 m. Therefore, it is necessary to ensure the stability of the rock mass destroyed in the shallow surrounding rock of the roadway and to strengthen the support for the shoulder corner of the roadway roof on the solid-coal side and coal pillar of Tailgate 8709.

Under a nonuniform stress field, when the lateral pressure coefficient is not equal to 1, the relationship between the radius r of the plastic zone of the roadway and the deviatoric stress difference can be calculated by the following formula [15]:

$$r = \sqrt{\frac{2a^2\gamma H \sin\varphi \cos 2\theta (1-\lambda)}{2C\cos\varphi + \gamma H(1+\lambda)\sin\varphi - (s_1 - s_3)}}, \quad (8)$$

where a is the equivalent radius of the roadway, taking the outer circle radius of the roadway as 2.65 m; γ is the bulk density of the rock, 25 kN/m^3; H is the buried depth of the roadway, 300 m; φ is the internal friction angle, 27°; λ is the coefficient of lateral pressure, 1.2; C is the cohesion, 0.9 MPa; s_1 is the maximum principal deviatoric stress, 6.98 MPa; s_3 is the minimum principal deviatoric stress, 1.51 MPa; θ is the angle of any point in the plane.

This formula shows that the maximum radius of the plastic zone of the circular roadway is 6.45 m at 10 m ahead of the N8709 coal face in No. 11 coal seam. The depth of the plastic zone of the roadway is 3.80 m after subtracting 2.65 m from the radius of circular roadway. The result from the formula is approximately consistent with the numerical simulation, verifying the plausibility of the simulation. Therefore, the distribution of deviatoric stress under the influence of multi-coal-seam mining is similar to the plastic zone in the surrounding rock of Tailgate 8709 in No. 11 coal seam.

4. Control Mechanism and Technology for the Surrounding Rock of Tailgate 8709

4.1. Analysis of Control Measures. Under multi-coal-seam mining, the peak zone of deviatoric stress and the plastic zone for the surrounding rock of Tailgate 8709 deflect to the shoulder corner of the roadway roof on the solid-coal side and to the bottom corner of the coal pillar. The plastic failure range of two corners of the roadway is large. When the advance coal face is 10 m ahead of Tailgate 8709, the depths of the plastic zone in the roof, solid-coal side, coal pillar, and floor are about 4.0 m, 3.0 m, 3.5 m, and 2.5 m, respectively, and the plastic zone of the shoulder corner of the roadway

roof on the solid-coal side extends up to 4.0 m. These corners are the key areas to control the surrounding rock of Tailgate 8709. In the support design process, it is necessary to strengthen the support such as anchor cables to the key control areas to prevent large deformation and damage of the surrounding rock in these areas [43]. The maximum distances of the peak zone of deviatoric stress are 4.0 m, 3.0 m, 4.0 m, and 2.5 m, respectively. The profiles of the peak zones of deviatoric stress and the plastic zone of Tailgate 8709 are shown in Figure 11.

Through a comprehensive analysis of profiles of the peak zone of deviatoric stress and the plastic zone of Tailgate 8709, it is determined that the roadway roof and the shoulder corner of the roadway roof (in solid-coal side and coal pillar) have a large range of damage, which are beyond the support range of ordinary bolts. The roadway roof takes the combined support of $\Phi 18 \times 2000$ mm bolts, $\Phi 17.8 \times 6300$ mm single-anchor cables, and truss anchor cables. The single-anchor cable in the shoulder corner of the roadway roof on the solid-coal side is arranged at an angle of 20° on the inclined solid-coal side. The bolt parameters on both sides of the roadway are $\Phi 18 \times 2000$ mm. $\Phi 17.8 \times 5000$ mm and $\Phi 17.8 \times 4000$ mm single-anchor cable are arranged anti-asymmetrically on the coal pillar downward with an incline of 15° from the horizontal, and on the solid-coal side upward with an incline of 15° from the horizontal.

4.2. Control Mechanisms for Surrounding Rock in Tailgate 8709

4.2.1. Mechanisms Using Combined Support by Bolts and Anchor Cables. The roof and two ribs in Tailgate 8709 take $\Phi 18 \times 2000$ mm thread steel bolts, which can connect the rock mass within the scope of shallow failure into a whole and enhance the integrity of the shallow roadway surrounding rock. The central anchor cable in the roof is arranged vertically, and the anchor cable in the shoulder corner of the roadway roof on the solid-coal side is arranged at an incline. At the same time, a single-anchor cable is inclined downward on the coal-pillar side and inclined upward on the solid-coal side passing through the peak zone of deviatoric stress. The high-strength and high pretension anchor cable can exert high-pressure stress on the roadway surrounding rock and using bolts can form a skeleton network structure in the pressure stress area. The anchor cable can tie the bearing structure formed by the bolts in the shallow surrounding rock to the deep stable rock strata. This makes the roof form a large-scale main bearing structure connected by the deep and shallow rocks and enhances the bearing capacity of the shallow surrounding rock of the roadway [44, 45], thereby effectively inhibiting the separation of roof strata and maintaining the integrity of the bending deformation process of the roadway roof.

4.2.2. Supporting Mechanisms Using a Truss Anchor Cable. A truss anchor cable is installed by two roof anchor cables at an incline at a place close to the two ribs. A certain preload is applied at the lower end of the anchor cable through a connector, so that the two anchor cables form a single bearing structure (Figure 11). The high pretension truss anchor cable system is used in the roadway roof to apply compound prestress to the regional roof fracture block and the rock mass above; this not only is beneficial to a roof in a state of multidirectional compressive stress but also improves the strength and deformation resistance of the coal and rock mass. It makes the surrounding rock within the anchorage range of the truss anchor cable consistent with the deformation of the upper rock mass and reduces the separation layer with the upper rock mass. At the same time, the truss anchor cable has a large length and strong shear resistance. The anchor cable in the two ribs of the roadway passes through the peak zone of deviatoric stress and the plastic zone and has a large range of action. It can effectively control the shear failure of the roof and the fracture of both sides of the layered roof structure and thus facilitates the balance of the overall structure of the anchoring zone [46].

4.3. Support Scheme of Tailgate 8709

4.3.1. Roof Support. The test roadway of this study is located at 350-470 m in Tailgate 8709. The roof is supported by threaded steel bolts, 18 mm in diameter and 2000 mm in length, with an interrow spacing of 1000 mm × 1000 mm. The roof bolts on the coal-pillar side are 750 mm away from the coal pillar and are installed at 70° from the horizontal. The bolts are connected by *W*-type steel strips of 3500 mm × 220 mm × 3 mm to form an integral bearing structure. The sizes of the steel pallets are 110 mm × 110 mm × 3 mm. High-strength and high pretension roof anchor cables, 17.8 mm in diameter, 6300 mm in length, and 1500 mm in array pitch, are installed at 55° from the horizontal on the solid-coal side to strengthen the support for the large-scale unstable rock in the roof corner. The roof support uses high-strength and high pretension anchor and truss anchor cables, 17.8 mm in diameter and 6300 mm in length. The single anchor cables are arranged between two rows of truss anchor cables with an array pitch of 4000 mm. The drilling depth of the single anchor cables, which are arranged vertically to the roof, is 6000 mm, while the drilling depth of the truss anchor cables, which have a pretension of at least 120 kN and are arranged at 20° to the vertical, is 5000 mm. In addition, the bottom span of the truss anchor cables is 2100 mm, and the distance between the borehole and solid coal rib is 1200 mm.

4.3.2. Rib Support. The two ribs are supported by threaded steel bolts, 18 mm in diameter and 2000 mm in length, with an interrow spacing of 800 mm × 1500 mm. The distance between the top bolts of the two ribs and roof is 800 mm, and the top and bottom rib bolts are installed at 10° from the horizontal. High-strength and high pretension rib anchor cables, 17.8 mm in diameter and 5000 mm in length, are installed at 20° downward from the horizontal in the coal pillar, while the high-strength and high pretension rib anchor cables, 17.8 mm in diameter and 4000 mm in length, are installed at 15° upward from the horizontal on the solid-coal

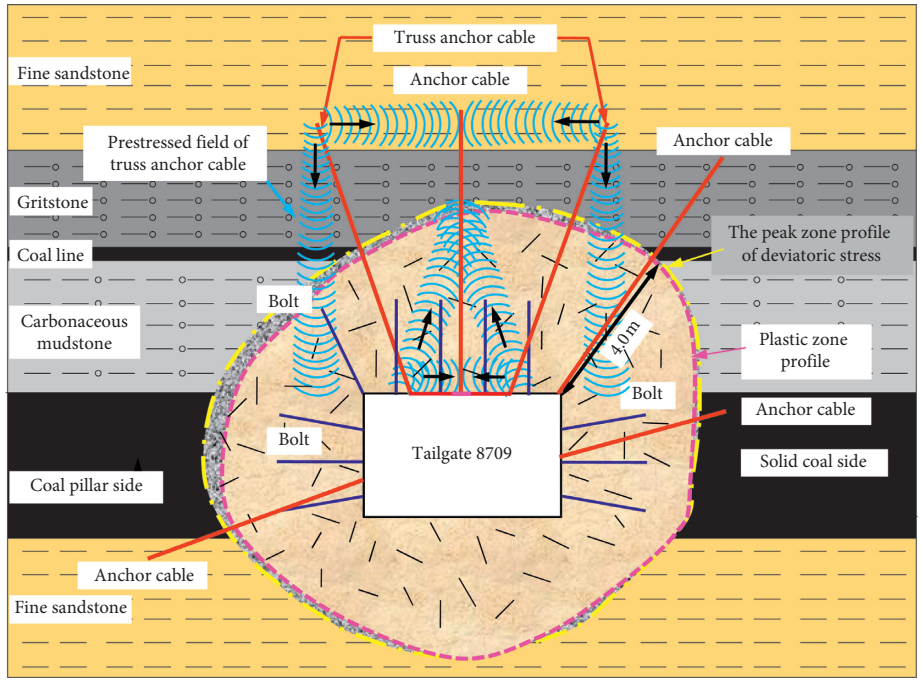

Figure 11: Profiles of peak zone of deviatoric stress and plastic zone of Tailgate 8709.

side. The rib-support anchor cables, with an array pitch of 1500 mm, could pass through the profiles of peak zone of deviatoric stress and the plastic zone, and the distance between the anchor cables (with steel pallets of 450 mm × 280 mm × 5 mm) and the roof is 1500 mm on the solid-coal side. The drilling diameter of all anchor cables and bolts in the above support is 28 mm, and the breaking load of anchor cables is 360 kN. The stereogram and planar graph of Tailgate 8709 support are shown in Figure 12.

To verify the accuracy of the plastic zone determined in numerical simulation and the practicability of the combined support technology for the surrounding rock around Tailgate 8709, a KDVJ-400 electronic drilling peep instrument [47–49] is used to observe the fracture zone development in the surrounding rock at the positions of the roof anchor cable in the roof corner, roof anchor cable on the coal-pillar side, and anchor cable in the coal pillar, as shown in Figure 12(b).

The carbonaceous mudstone at a depth of 0.2 m in the roof corner down the borehole is relatively fragmented, with massive longitudinal fractures, irregular fractures, and cavities. Furthermore, the opening degree of the fractures is relatively large, and the integrity of the rock is relatively poor, so that the hole can collapse easily in this region. At a depth of 0.2–1.8 m down the borehole, there are longitudinal fractures and a few small fractures in the rock mass indicating the relative development of fractures. The fractures in the carbonaceous mudstone at a depth of 1.8 m have obviously decreased compared with those at a depth of 0.2 m. At a depth of 1.8–2.8 m down the borehole, only 1-2 small longitudinal fractures are observed, which suggests that the rock mass tends to be stable in this region. At a depth of 4.3 m down the borehole, the rock mass has no joint or fracture, indicating the good integrity and stability of the rock mass. There are fractures of different degrees of development at a depth of 0–1.9 m down the borehole in the coal pillar, while the coal possesses relatively better integrity at a depth of 3.9 m. The rock mass is very fragmented, and the opening degree of the fractures is very large at the initial entrance of the borehole at the position of the roof anchor cable on the coal-pillar side, indicating that the integrity of the rock mass is relatively poor. Besides this, there are many kinds of irregular fractures at a depth of 0–1.8 m down the borehole; however, the fracture density decreases with depth down the borehole, and the rock mass gradually tends to stabilize in this region. Moreover, there are few fractures at a depth of 4.1 m, which indicates that the integrity of rock mass is better.

To summarize, according to drilling peep instrument results, the plastic zone profile is located between the intact rock mass and the failure rock mass, and the length of the anchor cable is greater than the range of the loose failure rock mass in the shallow surrounding rock of the roadway. Hence, the accuracy of the plastic zone of the roadway surrounding rock in the numerical simulation has been validated by drilling detection, and the anchor cable can pass through the loose failure rock mass in the shallow surrounding rock of Tailgate 8709, effectively anchoring it to the deep stable rock strata.

4.4. Results and Analysis of Mine Pressure Observation. In order to validate the control effects of combined support technology on the surrounding rock of Tailgate 8709 in No. 11 coal seam, the roof-to-floor convergences and rib-to-rib convergences of Tailgate 8709 have been monitored by an arrangement of monitoring stations; the observational results are shown in Figure 13. As shown in Figure 13(a), the roof-to-floor

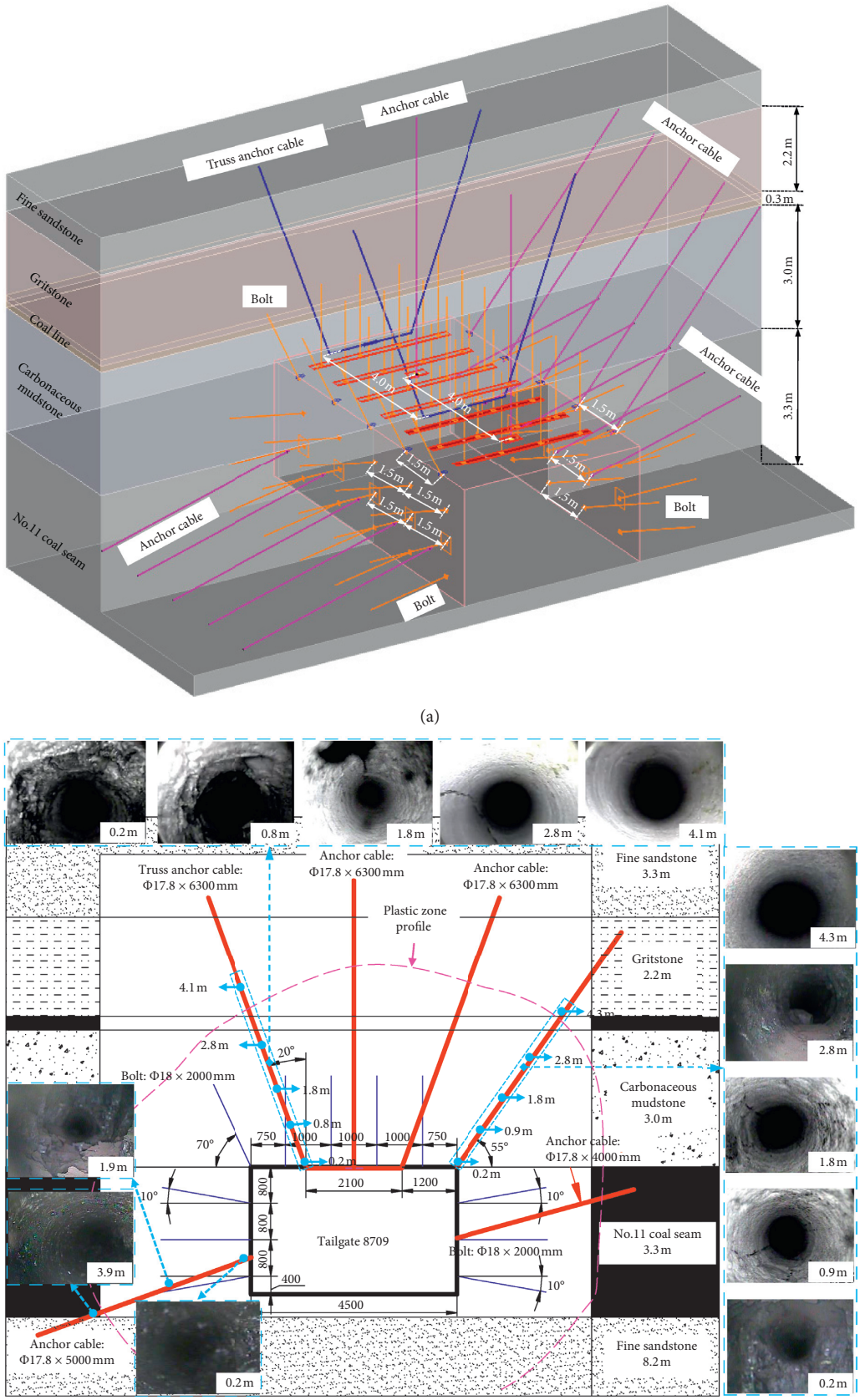

Figure 12: Support scheme of Tailgate 8709: (a) stereogram; (b) planar graph.

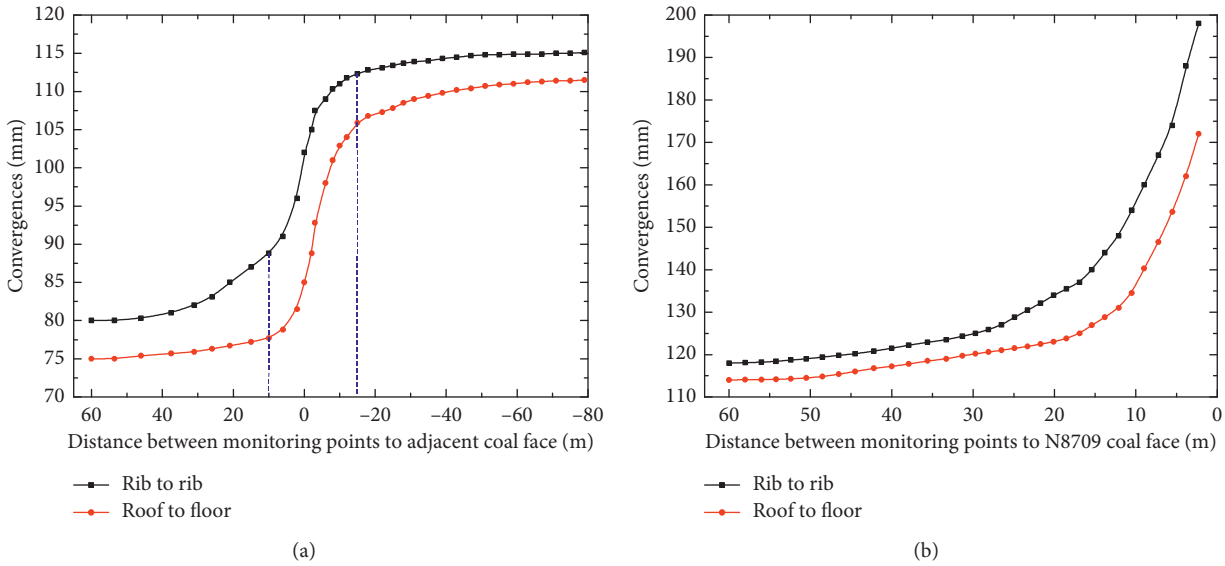

Figure 13: Results of mine pressure observation of Tailgate 8709 in No. 11 coal seam: (a) in the mining process of adjacent coal face; (b) in the mining process of the N8709 coal face.

convergences and rib-to-rib convergences of the Tailgate are 75 mm and 80 mm, respectively, without the mining-induced influence of the adjacent the N8707 coal face in No. 11 coal seam. When the adjacent coal face advance is 10 m ahead of the monitoring station, the roof-to-floor convergences and rib-to-rib convergences of the surrounding rock significantly increase. When the adjacent coal face advance is 10 m behind the monitoring station, the convergence rate of the surrounding rock is obviously reduced and the deformation slowly increases. The final roof-to-floor convergences and rib-to-rib convergences of Tailgate 8709 are 112 mm and 115 mm, respectively, and the deformation is controlled within a reasonable range. As shown in Figure 13(b), when the N8709 coal face advance is 30 m ahead of the monitoring station, the roof-to-floor convergences and rib-to-rib convergences of the surrounding rock gradually increase. When the coal face advance is 15 m ahead of the monitoring station, the convergence rate of the surrounding rock is obviously increased. This indicates that the Tailgate begins to be strongly influenced by the mining of the N8709 coal face, and the convergences of the surrounding rock linearly increase. The final roof-to-floor convergences and rib-to-rib convergences of the Tailgate are 172 mm and 198 mm, respectively. In addition, damage to support systems, such as the pullout and breakage of bolts and anchor cables, fails to take place in the field. Consequently, the combined support technology for Tailgate 8709 provides effective control of roadway surrounding-rock deformation under the disturbance of multi-coal-seam mining.

5. Conclusions

In this paper, the deviatoric stress nephograms, stress curves, and plastic zone of the surrounding rock of Tailgate 8709 in No. 11 coal seam under the disturbance of the mining of the N8707 and N8709 coal faces in No. 7-4 coal seam and the N8707 and N8709 coal faces in No. 11 coal seam have been studied. The deflection angles of the peak zone of deviatoric stress after mining of the coal faces have been determined. The profiles of the peak zone of deviatoric stress and the plastic zone have been drawn. A combined support technology using high-strength and high pretension anchor cables and truss anchor cables has been proposed. The accuracy of the calculated plastic zone of the surrounding rock and the reliability of the combined support technology have been verified through drilling detection and mine pressure observation. The main conclusions are as follows:

(1) After the mining of the N8707 coal face in No. 7-4 coal seam, the deviatoric stress of the surrounding rock of Tailgate 8709 in No. 11 coal seam has an approximately symmetrical distribution, which has low impact on the floor surrounding rock of the roadway. The mining of the N8709 coal face in No. 7-4 coal seam has a certain influence on the floor of Tailgate 8709, which results in the deflection of the peak zone of deviatoric stress in the shallow surrounding rock of the roadway.

(2) The results of numerical simulation show that the peak zone of deviatoric stress of Tailgate 8709 in No. 11 coal seam continuously deflects under multi-coal-seam mining. The peak zone of deviatoric stress in the roadway roof deflects by 34°, 13°, and 53° after the mining of the N8709 coal face in No. 7-4 coal seam and the N8707 coal face in No. 11 coal seam and in the advance 10 m of the N8709 coal face in No. 11 coal seam, respectively. This necessitates seeking a new effective bearing structure for the damaged surrounding rock. The supporting components such as anchor cables need to be anchored to the deep stable rock through the position of the peak zone of deviatoric stress.

(3) The nephogram pattern of deviatoric stress of the surrounding rock is consistent with the plastic zone in Tailgate 8709. The maximum plastic-zone depths under multi-coal-seam mining in the Tailgate 8709 roof, solid-coal side, coal pillar, and floor are about 4.0 m, 3.0 m, 3.5 m, and 2.5 m, respectively, and the plastic zone in the shoulder corner of the roadway on the solid-coal side extends up to 4.0 m. The corresponding peak zones of deviatoric stress are about 4.0 m, 3.0 m, 4.0 m, and 2.5 m away from the roadway surface. The maximum distance between the profiles of the peak zone of deviatoric stress and the plastic zone is not more than 1.0 m, and the plastic zone is large in the shoulder corner of the roadway roof in the solid-coal side and the coal pillar.

(4) Based on the analysis of profiles of the peak zone of deviatoric stress and the plastic zone of Tailgate 8709 under multi-coal-seam mining, a combined support technology based on high-strength and high pretension anchor cables and truss anchor cables is put forward. Long, inclined, high-strength anchor cables in the shoulder corner of the roadway roof on the solid-coal side and in the coal pillar and short, inclined anchor cables on the solid-coal side are suggested as a means of strengthening the support. The results of drilling detection and mine pressure observation show that the deformation of the surrounding rock in Tailgate 8709 has been effectively controlled. This research can provide a point of reference for roadway support under similar conditions.

Data Availability

Some data used to support the findings of this study are included within the article. Other data used to support the findings of this study are available from the corresponding author upon request.

Conflicts of Interest

The authors declare that there are no conflicts of interest related to the publication of this manuscript.

Authors' Contributions

Dongdong Chen, Shengrong Xie, and Fulian He conceived and designed the research. En Wang designed the model and the computational framework and wrote the paper. Long Wang was involved in the construction of numerical model. Qing Zhang and Xiaoyu Wu were involved in the numerical simulation. Zaisheng Jiang verified the analytical data. Yubo Li and Songhao Shi supplied the on-site data and verified the model in the on-site test.

Acknowledgments

This research was funded by the National Natural Science Foundation of China (Grant nos. 52004286, 51974317, and 52074296), the China Postdoctoral Science Foundation (Grant nos. 2020T130701 and 2019M650895), the Fundamental Research Funds for the Central Universities (Grant no. 2020YJSNY06), and the Yue Qi Young Scholar Project, China University of Mining & Technology, Beijing (Grant no. 800015Z1104). The authors would like to acknowledge the continuous support from Jinhuagong coal mine during the on-site sampling and monitoring.

References

[1] L.-Y. Zhang, K.-Z. Deng, C.-G. Zhu, and Z.-Q. Xing, "Analysis of stability of coal pillars with multi-coal seam strip mining," *Transactions of Nonferrous Metals Society of China*, vol. 21, no. 3, pp. S549–S555, 2011.

[2] W. Shen, L. M. Dou, H. He, and G. A. Zhu, "Rock burst assessment in multi-seam mining : a case study," *Arabian Journal of Geosciences*, vol. 10, no. 8, p. 196, 2017.

[3] L. S. Song, S. K. Zhao, J. Liu, X. Z. Wei, R. J. Han, and H. B. Jiang, "Experimental research on rules of rock burst tendency evolution and mechanical properties of "roof-coal" structure body," *Journal of China Coal Society*, vol. 39, no. S1, pp. 23–30, 2014.

[4] H. Liu, J. Dai, J. Q. Jiang, P. Wang, and J. Q. Yang, "Analysis of overburden structure and pressure-relief effect of hard roof blasting and cutting," *Advances in Civil Engineering*, vol. 2019, Article ID 1354652, 14 pages, 2019.

[5] B. Yu, "Structural evolution of breaking roof group of multiple coal seams and its influence on lower coal seam mining," *Journal of China Coal Society*, vol. 40, no. 2, pp. 261–266, 2015.

[6] D. Zhu, X. Song, H. Li, Z. Liu, C. Wang, and Y. Huo, "Cooperative load-bearing characteristics of a pillar group and a gob pile in partially caved areas at shallow depth," *Energy Science & Engineering*, vol. 8, no. 1, pp. 89–103, 2020.

[7] Y. L. Tan, X. S. Liu, J. G. Ning, and Y. W. Lu, "In situ investigations on failure evolution of overlying strata induced by mining multiple coal seams," *Geotechnical Testing Journal*, vol. 40, no. 2, pp. 244–257, 2017.

[8] J. Li, Y. Huang, J. Zhang, M. Li, M. Qiao, and F. Wang, "The influences of key strata compound breakage on the overlying strata movement and strata pressure behavior in fully mechanized caving mining of shallow and extremely thick seams: a case study," *Advances in Civil Engineering*, vol. 2019, Article ID 5929635, 11 pages, 2019.

[9] W. Qiang, L. Yuanzhang, and Y. Liu, "Using the vulnerable index method to assess the likelihood of a water inrush through the floor of a multi-seam coal mine in China," *Mine Water and the Environment*, vol. 30, no. 1, pp. 54–60, 2011.

[10] P. Zhang, B. Tulu, M. Sears, and J. Trackemas, "Geotechnical considerations for concurrent pillar recovery in close-distance multiple seams," *International Journal of Mining Science and Technology*, vol. 28, no. 1, pp. 21–27, 2018.

[11] C. V. Deutsch and B. J. Wilde, "Modeling multiple coal seams using signed distance functions and global kriging," *International Journal of Coal Geology*, vol. 112, no. S1, pp. 87–93, 2013.

[12] H. Shang, J. Ning, S. Hu, S. Yang, and P. Qiu, "Field and numerical investigations of gateroad system failure under an irregular residual coal pillar in close-distance coal seams," *Energy Science & Engineering*, vol. 7, no. 6, pp. 2720–2740, 2019.

[13] Y. Yuan, W. J. Wang, S. Q. Li, and Y. J. Zhu, "Failure mechanism for surrounding rock of deep circular roadway in

coal mine based on mining-induced plastic zone," *Advances in Civil Engineering*, vol. 2018, Article ID 1835381, 14 pages, 2018.

[14] G. H. Deng, S. J. Shao, C. L. Chen, and F. T. She, "A structural parameter reflecting coupling action between shear stress and spherical stress," *Rock and Soil Mechanics*, vol. 33, no. 8, pp. 2310–2314, 2012.

[15] N. J. Ma, J. Li, and Z. Q. Zhao, "Distribution of the deviatoric stress field and plastic zone in circular roadway surrounding rock," *Journal of China University of Mining and Technology*, vol. 44, no. 2, pp. 206–213, 2015.

[16] L. Xu, H. X. Wei, Z. Y. Xiao, and B. Li, "Engineering cases and characteristics of deviatoric stress under coal pillar in regional floor," *Rock and Soil Mechanics*, vol. 36, no. 2, pp. 561–568, 2015.

[17] L. Xu, H. K. Wu, B. Li, and T. Q. Xiao, "Stability and control of surrounding rock in ultra-high roadway," *Chinese Journal of Rock Mechanics and Engineering*, vol. 33, no. S2, pp. 3891–3902, 2014.

[18] W. J. Yu, G. S. Wu, C. Yuan, P. Wang, and S. H. Du, "Failure characteristics and engineering stability control of roadway surrounding rock based on deviatoric stress field," *Journal of China Coal Society*, vol. 42, no. 6, pp. 1408–1419, 2017.

[19] F. L. He, L. Xu, H. K. Wu, and T. D. Li, "Deviatoric stress transfer and stability of surrounding rock in large-section open-off cut roof," *Chinese Journal of Geotechnical Engineering*, vol. 36, no. 6, pp. 1122–1128, 2014.

[20] S. R. Xie, S. S. Yue, D. D. Chen et al., "Deviatoric stress evolution laws and control of surrounding rock at gob-side entry retaining in deep backfilling mining," *Journal of China Coal Society*, vol. 43, no. 7, pp. 1837–1846, 2018.

[21] S. R. Xie, L. Xu, G. C. Zhang, S. J. Li, S. Gong, and L. G. Yang, "Subsidence broken of deep gob-side entry retaining surrounding rock structure with large mining height and its control," *Rock and Soil Mechanics*, vol. 36, no. 2, pp. 569–575, 2015.

[22] H. Wu, X. Wang, W. Wang, G. Peng, and Z. Zhang, "Deformation characteristics and mechanism of deep subsize coal pillar of the tilted stratum," *Energy Science & Engineering*, vol. 8, no. 2, pp. 544–561, 2020.

[23] S.-L. Wang, S.-P. Hao, Y. Chen, J.-B. Bai, X.-Y. Wang, and Y. Xu, "Numerical investigation of coal pillar failure under simultaneous static and dynamic loading," *International Journal of Rock Mechanics and Mining Sciences*, vol. 84, pp. 59–68, 2016.

[24] W. F. Li, J. B. Bai, S. Peng, X. Y. Wang, and Y. Xu, "Numerical modeling for yield pillar design: a case study," *Rock Mechanics and Rock Engineering*, vol. 48, no. 1, pp. 305–318, 2015.

[25] Z. Zhang, J. Bai, Y. Chen, and S. Yan, "An innovative approach for gob-side entry retaining in highly gassy fully-mechanized longwall top-coal caving," *International Journal of Rock Mechanics and Mining Sciences*, vol. 80, pp. 1–11, 2015.

[26] H. Wang, Y. Jiang, Y. Zhao, J. Zhu, and S. Liu, "Numerical investigation of the dynamic mechanical state of a coal pillar during longwall mining panel extraction," *Rock Mechanics and Rock Engineering*, vol. 46, no. 5, pp. 1211–1221, 2013.

[27] S. Yan, J. Bai, X. Wang, and L. Huo, "An innovative approach for gateroad layout in highly gassy longwall top coal caving," *International Journal of Rock Mechanics and Mining Sciences*, vol. 59, pp. 33–41, 2013.

[28] R. Singh, S. K. Singh, A. Kushwaha, and A. Sinha, "Stability of the parting between coal pillar workings in level contiguous seams during depillaring," *International Journal of Rock Mechanics and Mining Sciences*, vol. 55, pp. 1–14, 2012.

[29] H. Wang, B. A. Poulsen, B. Shen, S. Xue, and Y. Jiang, "The influence of roadway backfill on the coal pillar strength by numerical investigation," *International Journal of Rock Mechanics and Mining Sciences*, vol. 48, no. 3, pp. 443–450, 2011.

[30] J. W. Zhou, W. Y. Xu, M. W. Li, X. Q. Zhou, and C. Shi, "Application of rock strain softening model to numerical analysis of deep tunnel," *Chinese Journal of Rock Mechanics and Engineering*, vol. 28, no. 6, pp. 1116–1127, 2009.

[31] Y. D. Jiang, H. W. Wang, Y. X. Zhao, C. H. Liu, and X. L. Zhu, "Study of complementary supporting technology of extremely soft rock mining roadway," *Chinese Journal of Rock Mechanics and Engineering*, vol. 28, no. 12, pp. 2383–2390, 2009.

[32] X. M. Sun, Y. Y. Liu, J. W. Wang, J. B. Li, S. J. Sun, and X. B. Cui, "Study on three-dimensional stress field of gob-side entry retaining by roof cutting without pillar under near-group coal seam mining," *Processes*, vol. 7, no. 9, p. 522, 2019.

[33] X. Dong, A. Karrech, H. Basarir, M. Elchalakani, and A. Seibi, "Energy dissipation and storage in underground mining operations," *Rock Mechanics and Rock Engineering*, vol. 52, no. 1, pp. 229–245, 2019.

[34] J. Fang, L. Tian, Y. Y. Cai, Z. G. Cao, J. H. Wen, and Z. J. Wen, "A mechanical model of the overlying rock masses in undersea coal mining and a stress-seepage coupling numerical simulation," *Advances in Civil Engineering*, vol. 2018, Article ID 8161498, 14 pages, 2018.

[35] H. Kang, J. Lou, F. Gao, J. Yang, and J. Li, "A physical and numerical investigation of sudden massive roof collapse during longwall coal retreat mining," *International Journal of Coal Geology*, vol. 188, pp. 25–36, 2018.

[36] X. S. Zhang, H. C. Yu, J. Y. Dong et al., "A physical and numerical model-based research on the subsidence features of overlying strata caused by coal mining in Henan, China," *Environmental Earth Sciences*, vol. 76, no. 20, p. 705, 2017.

[37] D. Y. Qian, N. Zhang, H. Shimada, C. Wang, T. Sasaoka, and N. C. Zhang, "Stability of goaf-side entry driving in 800-m-deep island longwall coal face in underground coal mine," *Arabian Journal of Geosciences*, vol. 9, no. 1, p. 82, 2016.

[38] F. Gao, D. Stead, and H. Kang, "Numerical simulation of squeezing failure in a coal mine roadway due to mining-induced stresses," *Rock Mechanics and Rock Engineering*, vol. 48, no. 4, pp. 1635–1645, 2015.

[39] M. Zhang, H. Shimada, T. Sasaoka, K. Matsui, and L. Dou, "Evolution and effect of the stress concentration and rock failure in the deep multi-seam coal mining," *Environmental Earth Sciences*, vol. 72, no. 3, pp. 629–643, 2014.

[40] T. P. Medhurst and E. T. Brown, "A study of the mechanical behaviour of coal for pillar design," *International Journal of Rock Mechanics and Mining Sciences*, vol. 35, no. 8, pp. 1087–1105, 1998.

[41] P. F. He, P. H. S. W. Kulatilake, D. Q. Liu, and M. C. He, "Development of new three-dimensional coal mass strength criterion," *International Journal of Geomechanics*, vol. 17, no. 3, 20 pages, Article ID 04016067, 2016.

[42] Q. Feng, J. C. Fan, Q. Zhang, and B. S. Jiang, "Elastoplastic analysis of spherical cavity in strain-softening rock masses based on Mohr-Coulomb criterion," *Journal of China Coal Society*, vol. 39, no. 5, pp. 836–840, 2014.

[43] W. J. Yu, B. Pan, F. Zhang, S. F. Yao, and F. F. Liu, "Deformation characteristics and determination of optimum supporting time of alteration rock mass in deep mine," *KSCE Journal of Civil Engineering*, vol. 11, no. 23, pp. 4921–4932, 2019.

[44] D. Fan, X. Liu, Y. Tan, L. Yan, S. Song, and J. Ning, "An innovative approach for gob-side entry retaining in deep coal

mines: a case study," *Energy Science & Engineering*, vol. 7, no. 6, pp. 2321–2335, 2019.

[45] S. R. Xie, E. Wang, D. D. Chen et al., "Failure analysis and control mechanism of gob-side entry retention with a 1.7–m flexible-formwork concrete wall: a case study," *Engineering Failure Analysis*, vol. 117, no. 22, p. 16, Article ID 104816, 2020.

[46] Y. Tai, H. C. Xia, X. B. Meng, and F. J. Kuang, "Failure mechanism of the large-section roadway under mined zones in the ultra-thick coal seam and its control technology," *Energy Science and Engineering*, vol. 8, no. 8, pp. 1–16, 2019.

[47] W. J. Yu and F. F. Liu, "Stability of close chambers surrounding rock in deep and comprehensive control technology," *Advances in Civil Engineering*, vol. 2018, Article ID 6275941, 18 pages, 2018.

[48] J. Wang, J. Ning, L. Jiang, J. Q. Jiang, and T. Bu, "Structural characteristics of strata overlying of a fully mechanized longwall face: a case study," *Journal of the South African Institute of Mining and Metallurgy*, vol. 118, no. 11, pp. 1195–1204, 2018.

[49] Z. Xie, N. Zhang, D. Qian, C. Han, Y. An, and Y. Wang, "Rapid excavation and stability control of deep roadways for an underground coal mine with high production in inner Mongolia," *Sustainability*, vol. 10, no. 4, p. 1160, 2018.